HaloSat Background Analysis

Jesse Bluem, Philip Kaaret, Lorella Angelini

November 2022

1 Summary

The document describes a new study of the particle-induced instrumental background of HaloSat and how to account for this when fitting Halosat spectra. The details motivating a reanalysis of the HaloSat background and the analysis that went into determining the parameters is described in the following sections. We find that the particle-induced instrumental background is best modeled as two power laws (Xspec model `powerlaw`). The main (hard) background power law is fit with a shallower fixed photon index around 0.7 (the values are slightly different for each detector and vary with the hard rate cut used) that contributes strongly across all energies. The values for the standard HaloSat hard rate cuts can be found in Table 1 (note that some fields in the HaloSat archive use nonstandard cuts). The secondary (soft) power law is a steeper component that primarily contributes at the lowest energies and has a fixed photon index of 3.4 for each detector. The background level varies between the individual detectors due to their different locations on the spacecraft (the detectors are referred to as D14, D54, and D38) and between observations, and as such the power law normalization must be fit separately for each detector in each set of spectra. These background components only use the diagonal HaloSat response matrix (hs_sdd_diag20180701v001.rmf) since they are particle induced events. The secondary softer power law should have the normalization fit alongside the fitting of the astrophysical parameters of interest, although it might exhibit degeneracy with complex models. Some individual fields might not find a significant contribution from the secondary low-energy power law. The main harder power law can also be fit alongside the secondary power law and the astrophysical parameters over the full 0.4-7 keV energy band. Alternatively, the normalization of the main power law can be determined by fitting that parameter alone to only the higher energies (above 2 or 3 keV), with all other parameter normalizations fixed to zero, assuming that no astrophysical sources infringe on this energy range. This can be done for each separate detector at the same time. An example script for loading and fitting HaloSat spectra can be found in Section 5.

2 Problems with the original background model

Previous studies of the HaloSat instrumental background used a single power law model folded through a diagonal response matrix without the photon redistribution function or photon effective area (Kaaret,

Hard rate cut	D14 photon index	D54 photon index	D38 photon index
0.12 c/s	0.80 ± 0.08	0.75 ± 0.08	0.73 ± 0.07
0.16 c/s	0.69 ± 0.06	0.65 ± 0.06	0.64 ± 0.07

Table 1: Photon indices for the primary background power law. The first column lists the standard hard rate cut level (data intervals with rates above the cut levels are removed) and the other columns are the photon indices for each detector. These values are medians based on fitting the fields from Bluem et al (2022), with median absolute error. Outliers identified with different colors in Figures 6 and 7 have been removed for the median calculation. These median values for the selected hard rate cut level should be used as fixed parameters in the spectral fit. These values should not be used with non-standard cuts.

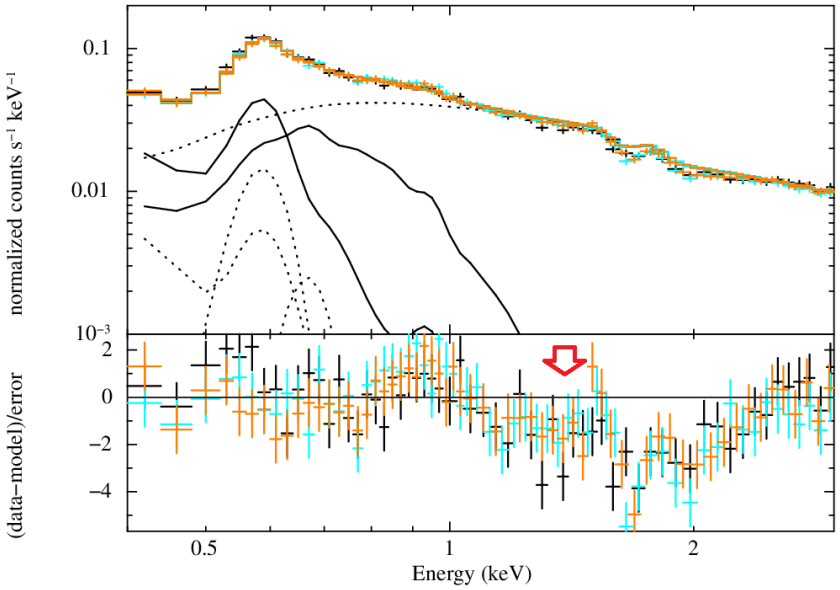

Figure 1: Three early background subtracted stacked spectra (one for each detector). The background subtracted here consists of single power law backgrounds for the contributing fields, summed as counts per spectral channels. The red arrow marks a significant over-subtraction in the middle energies that also manifests at higher energies as a sloped residual.

P. Feb 2021, https://heasarc.gsfc.nasa.gov/docs/halosat/analysis/back20210209.pdf). The recent HaloSat study of the circumgalactic medium (CGM), which stacked spectra from individual fields into a set of three high-statistics spectra, discovered that the previous background model was insufficient (Bluem et al. 2022). The initial method used to stack the spectra was to subtract the instrumental background from each field included in the study before stacking all the spectra from the different fields. Variations on the stacked spectra consistently exhibited a residual in the spectral fit shown as a deficit in counts in the middle energies (1.5-2.5 keV, see Figure 1). This region is dominated by the cosmic X-ray background (CXB). As the shape of the CXB spectrum is well understood, and any significant problem in the instrumental response would have been noticed in analyses of bright sources like the Crab, a problem in the instrumental background model is the obvious culprit.

At first glance, it appeared that the photon index of the background power law was incorrect. Changing the index, to overcome the 1.5-2.5 keV deficit, results in shifting the problems to the lower energies of the spectra, causing an excess of counts above the astrophysical model describing the emission sources. A similar residual at lower energy (0.4-0.5 keV) has been seen to varying degrees in other individual HaloSat observations, but the inconsistent nature of this excess emission had caused it to remain previously unidentified. The background over-subtraction in the middle of the spectra is consistent with an unfit low-energy excess skewing the fitted background power law, tilting it up towards the lower energies.

Due to this inconsistency, a different approach to stacking spectra was adopted - spectra from the individual fields were stacked without performing the background subtraction. The analysis of the three stacked spectra allowed us to identify the low-energy excess as a secondary background power law, fitting with a steep photon index of 3.4. The stacked spectra and best fit from Bluem et al. (2022) can be seen in Figure 2. The best fit model parameters are listed in Table 2. Due to entanglement of the additional background power law at low energy with peak astrophysical source emission in the same energy range, we recommend fixing the photon index for this component to 3.4 for individual fields, which mostly lack the depth of data to rigorously fit this parameter. In conclusion, the particle-induced instrumental background may be modelled by two power laws. The first power law is analogous to the background fitting described in the Kaaret Feb 2021 memo, while the second power law has a fixed photon index of 3.4.

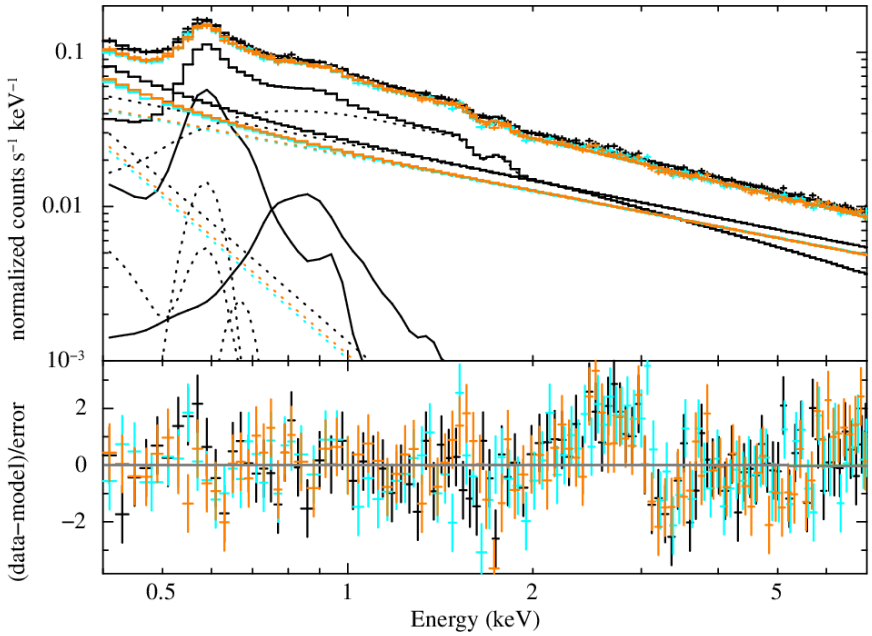

Figure 2: The stacked spectra from Bluem et al. (2022). Each HaloSat detector's spectrum is a different color. The spectra have two components for the CGM, marked with solid black lines. Foreground and background components are marked with dashed lines. The instrument backgrounds are the two linear components, which can be seen with separate normalizations for the three detectors. The summed background contributions can be seen as the sweeping solid colored lines crossing the figure. The discontinuity at 3 keV is from the high-energy count rate cuts used and unrelated to the background (see Section 4).

model	parameter	value
Warm CGM APEC	kT (keV)	0.166 ± 0.005
	EM ($\mathrm{cm}^{-6}\,\mathrm{pc}$)	$0.0129^{+0.0009}_{-0.0008}$
Hot CGM APEC	kT (keV)	$0.69^{+0.04}_{-0.05}$
	EM ($\mathrm{cm}^{-6}\,\mathrm{pc}$)	0.0013 ± 0.0002
Power law 1 (DPU 14)	photon index	0.79 ± 0.03
	normalization	$0.0254^{+0.0009}_{-0.0013}$
Power law 1 (DPU 54)	photon index	0.77 ± 0.03
	normalization	$0.0214^{+0.0008}_{-0.0011}$
Power law 1 (DPU 38)	photon index	0.76 ± 0.03
	normalization	$0.0211^{+0.0008}_{-0.0010}$
Power law 2	photon index	$3.4^{+1.0}_{-0.8}$
	normalization (DPU 14)	$0.0014^{+0.0018}_{-0.0008}$
	normalization (DPU 54)	$0.0011^{+0.0015}_{-0.0007}$
	normalization (DPU 38)	$0.0011^{+0.0013}_{-0.0006}$
Fit (DPU 14)	χ^2	359
Fit (DPU 54)	χ^2	369
Fit (DPU 38)	χ^2	341
Fit total	χ^2/DoF	1069/973

Table 2: Parameters of the model fitted to the stacked spectra in Figure 2. Column 1 is the name of the model component. Column 2 is the name of the parameters for the component. Column 3 is the value for the listed parameter. The top section includes the astrophysical components while the middle section includes the instrumental components, and the bottom section includes the fit statistics. Errors are the 90% confidence interval. This data used the 0.12 c/s hard rate cut. Note that this analysis used fitted photon indices, but the indices are consistent with the median values from Table 1.

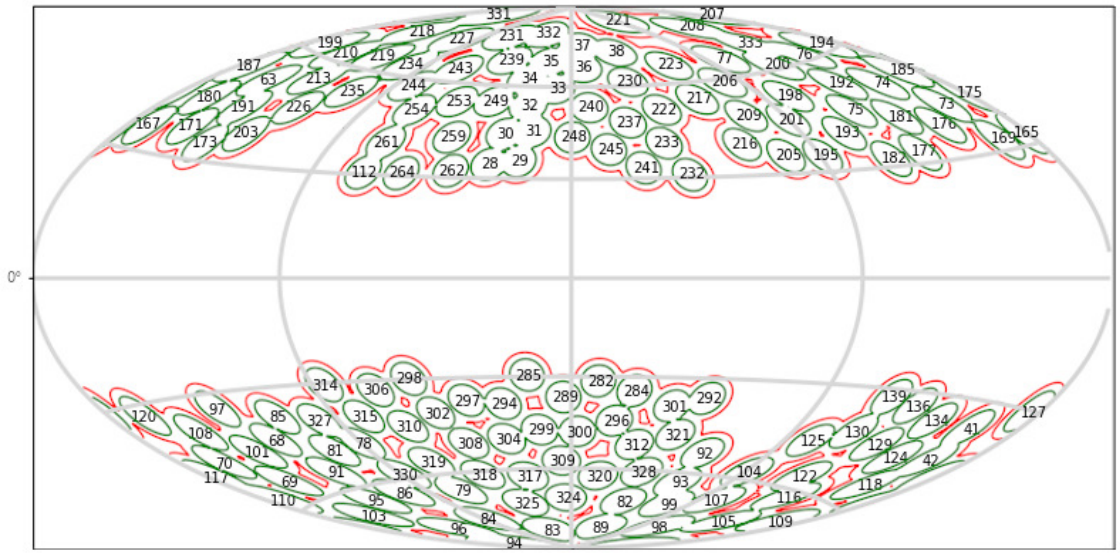

Figure 3: A map of the HaloSat fields studied in Bluem et al. (2022). These are the same fields utilized for this background study.

3 Individual field analysis

In the previous section we concluded that to fit the set of stacked spectra it is necessary to add an additional low energy power law that we attributed to the instrumental background and not to emission from an astrophysical source. Both background power laws vary between observations of the same field at different times, indicating that they are instrumental background components and not astrophysical sources. To further study and validate the background model, we applied the two power laws background method to all 156 individual fields in the CGM data set from Bluem et al. (2022), using an automated PyXspec pipeline. These fields were selected based on being 30 degrees or further away from the Galactic plane, alongside a Sun angle selection of greater than or equal to 110 degrees, to minimize effects from solar wind charge exchange (see Kuntz 2019 for more details). All fields used a count rate cut on the HaloSat hard band (defined as the 3-7 keV band) of 0.12 c/s and a count rate cut on the HaloSat VLE (very large event) band ($\geq$ 7 keV) of 0.75 c/s, removing time intervals with rates exceeding these cut thresholds. Fields below 5000 seconds of remaining data per detector, after the 0.12 c/s hard rate cut, were also removed. The same data set was studied with a hard rate cut of 0.16 c/s, using the same set of fields left after all 0.12 c/s selections were performed. The rates of 0.12 c/s and 0.16 c/s are the HaloSat standard hard rate cuts (the HaloSat data archive uses the standard 0.16 c/s cut rate for most fields, although some fields use non-standard hard rate cuts not covered in this background note). This is a larger sample of HaloSat fields than were used in the original HaloSat background analysis note. A map of the fields used can be seen in Figure 3.

These fields, with the 0.12 c/s hard rate cut, were fit with the refined background model and astrophysical model in Bluem et al. (2022). Figure 4 shows a plot of the hard rate versus the photon index of the main background power law. The correlation previously seen in the original HaloSat background analysis no longer appears. Studying other parameters derived for this data set reveals that the normalization of this main background power law is still strongly correlated with hard rate (Figure 5). This suggests that the previously observed correlation between photon index and hard rate was an effect of fitting a single power law instead of two power laws with fixed indices and normalizations that varied at different rates based on the observation hard rate. This effect can essentially be seen in Figure 2. If the normalization of the hard background power law is increased, due to a higher hard rate, the resulting fitted photon index becomes shallower. This was the exact trend observed in the previous background analysis note. Since there is no correlation between hard rate and photon index, a fixed value for photon index can be used. The fitted photon indices exhibit an asymmetric distribution, so the median values were used to determine the best photon index value to use. These parameter values are listed in Table 1. The photon index is different for each detector and changes

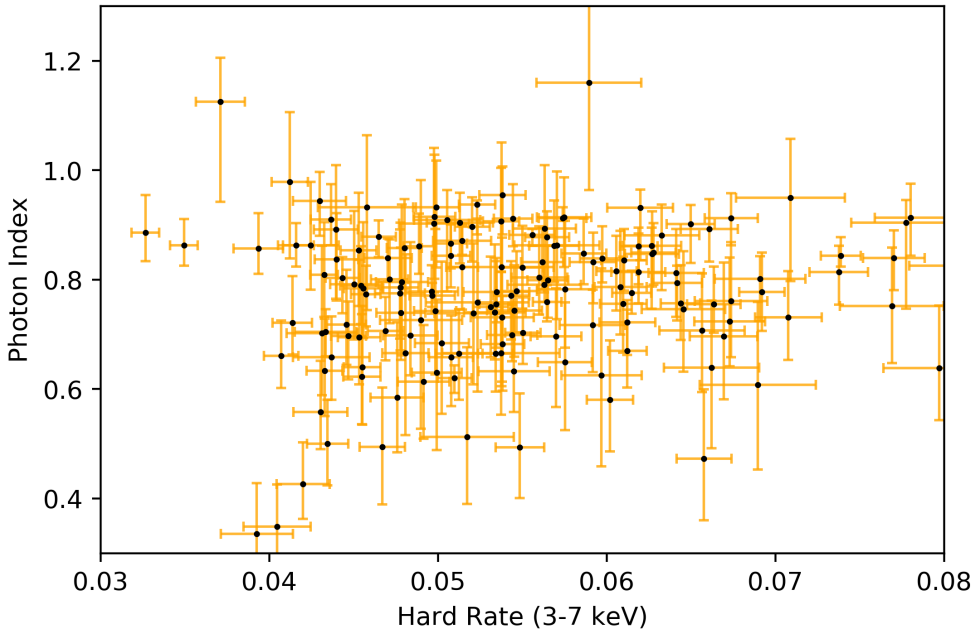

Figure 4: Photon index of the main background power law for DPU 14 versus hard rate for the total spectrum of the field. This is for a hard rate cut of 0.12 c/s. There is no observed correlation between hard rate and photon index, unlike the previous HaloSat background model.

based on the hard rate rate cut applied to the spectra. An example fit using the fixed photon indices on an individual field can be seen in Figure 6.

To test the fixed photon index fit, both cut rate data sets were refit using the median photon indices for each detector and the Cash statistic of the fits were compared. The results can be seen in Figure 7. For both cut levels, the overall trend is very consistent, with minimal shift in the Cash statistic when the photon indices are fixed to median values.

Many of the larger outliers in Figure 7 exhibit astrophysical emission more complicated than the standard spectral model used for this study. One possible consequence of these complicated spectra is that unfit emission can be included in the background fit by PyXspec, especially in the case where the background model is allowed to fit the photon index. The main source of these complicated spectra is the North Polar Spur (NPS) fields, marked in cyan in Figure 7. Another problematic field is HS0333, which is marked in magenta in Figure 7. HS0333 has a known bright source and exhibits significant residuals when fit with fixed photon indices. As such, we find that the fixed photon indices are good, and the two power laws background model is preferred. Table 1 includes the median values for the fitted photon indices, with the aforementioned outliers removed, which are the preferred values for fixed photon indices. Note that the fits used to generate Figure 7 used medians based on the entire data set including the outliers. This does not have a significant effect on the fits in Figure 7 since the median values only change slightly with the removal of outliers, and the change is much smaller than the individual photon index error when it is allowed to fit.

Figure 8 compares the resulting CGM temperatures from the model fits for each method. Figure 9 compares the normalizations for the same CGM model components. For most fields the parameter values do not change significantly. The most notable changes occurred in fields that initially fit with atypical temperatures when the background photon index was free to fit, which were moved closer to the center of the distribution when the background photon index is fixed during fitting. These were predominately due to local minima caused by degeneracy with the background when the photon index is allowed to be fit.

In conclusion, the suggested fitting method for the HaloSat instrumental background is to use two power laws with the diagonal response matrix. The main hard power law uses a fixed photon index, separate for each detector, from Table 1. These indexes are specific to the hard rate cut used, and the indexes in Table 1 only apply to the two standard cuts used with the HaloSat data. The secondary softer power law uses a

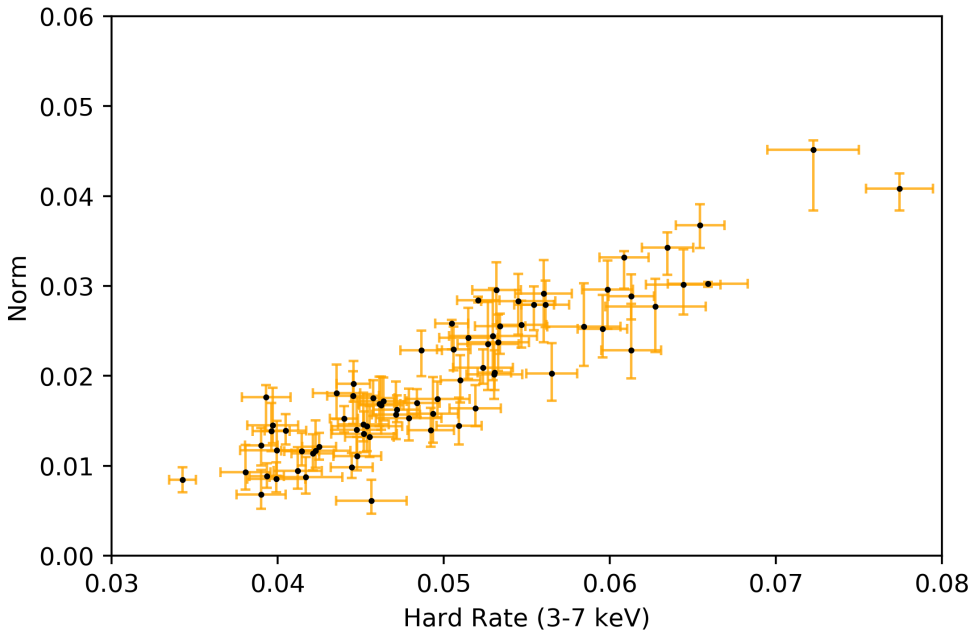

Figure 5: Normalization of the main background power law versus hard rate for detector D38. Only fields from the southern hemisphere are shown in this example.

fixed photon index of 3.4 for each detector. The normalizations of both components are left free to fit and remain unlinked between the detectors. The 3.4 photon index power law component varies enough that at times it is not required. In these cases, the best fit gives a normalization that is consistent with zero. The 3.4 photon index component can also be degenerate with astrophysical model components in some complex fields.

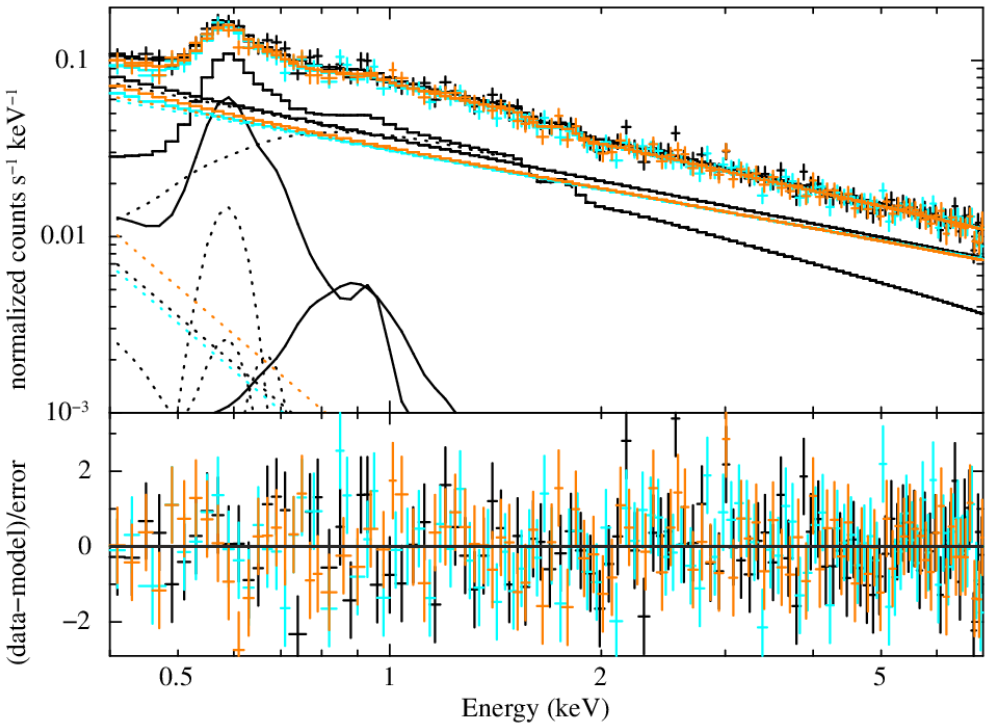

Figure 6: Example fit for a HaloSat field (HS0319, 0.16 c/s hard rate cut). Each detector is a different color. Line styles follow Figure 2. This field has a weak secondary power law normalization.

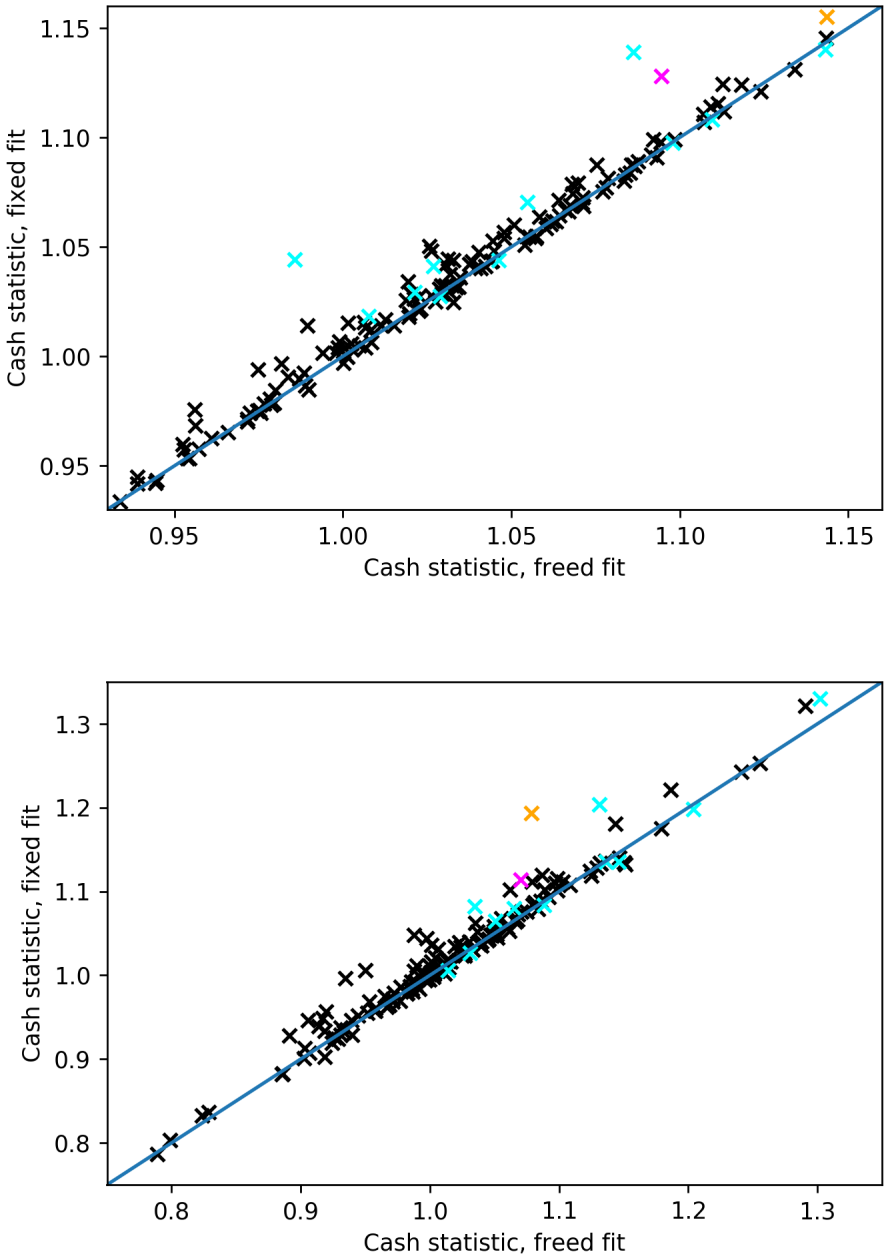

Figure 7: Cash fit statistic difference between fitting the photon index of the main background power law (x-axis) and freezing it to the median value for the full CGM data set (y-axis). NPS fields are marked in cyan. HS0223 is low data and marked in orange. HS0333 has a known bright source that is unfit in the spectrum and is marked in magenta. The top figure is for the 0.16 c/s hard rate cut and the bottom is for the 0.12 c/s hard rate cut.

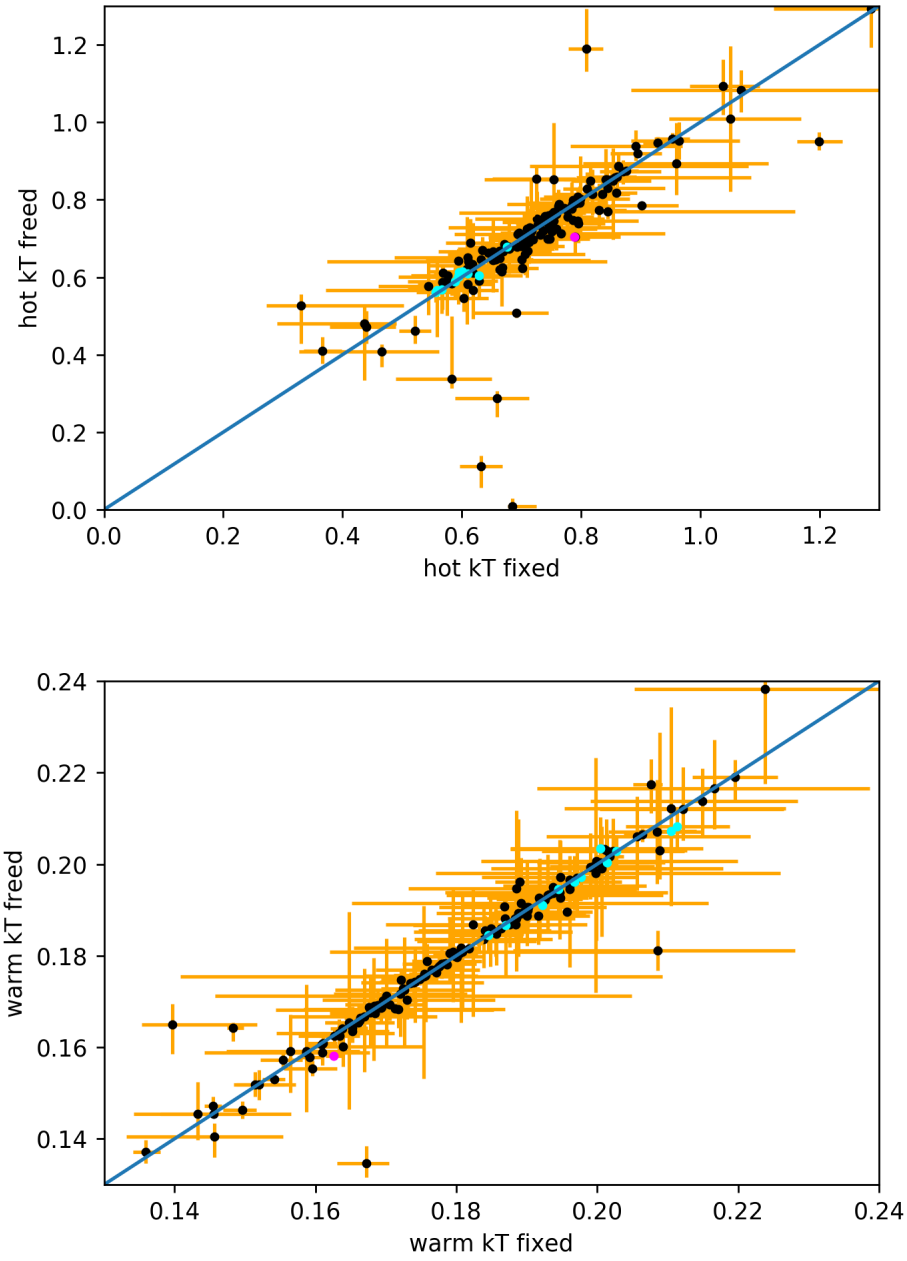

Figure 8: Temperature of the hot (top) and warm (bottom) CGM components for a fit with a free-to-fit background photon index versus a fit with the fixed photon index. This is for the 0.12 c/s hard rate cut and all errors are 90% confidence intervals. Fields are marked with different colors following Figure 7. Most fields are consistent between the two fits, while some atypical high and low temperature CGM hot component fields have moved closer to the center of the distribution with a fixed photon index. These are predominately due to local minima in the fits with freed indexes.

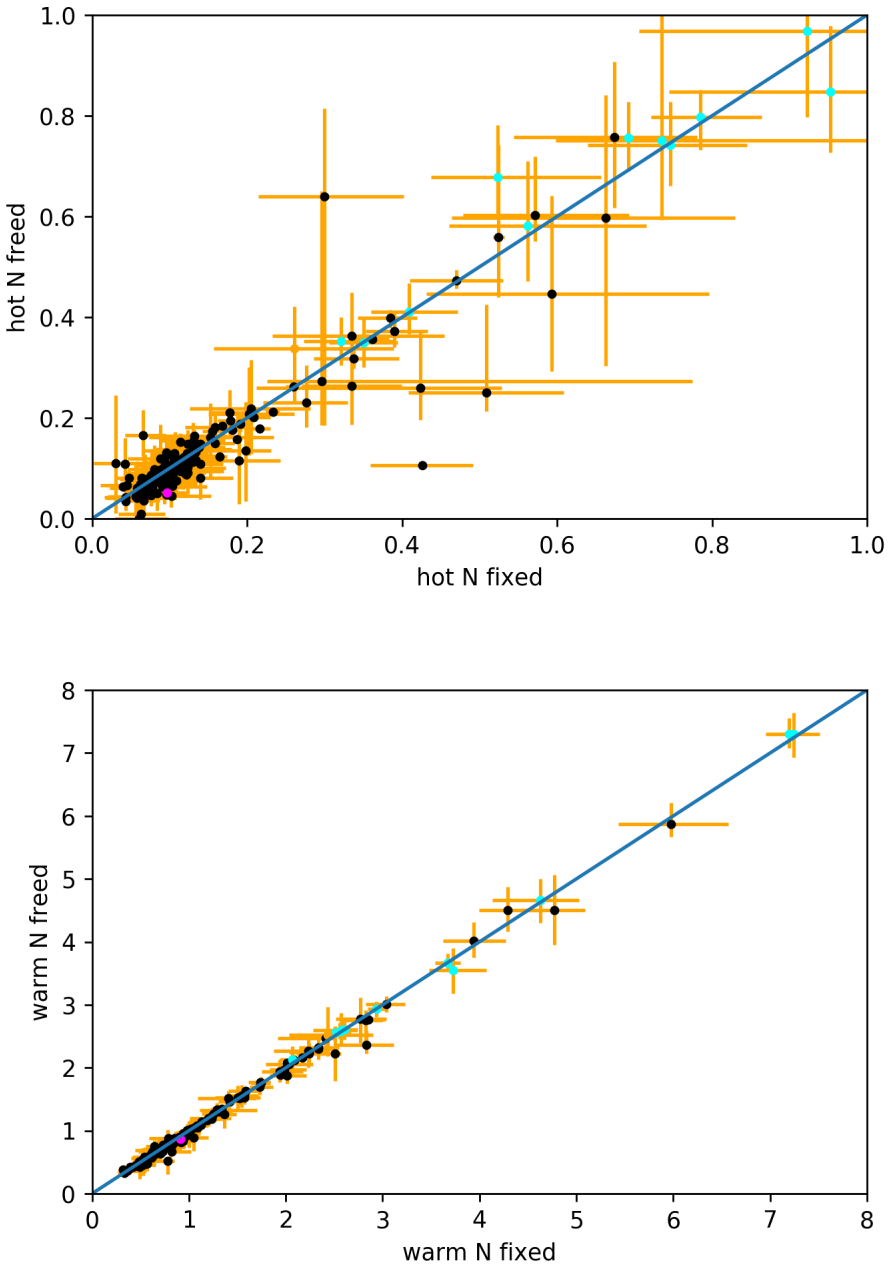

Figure 9: Normalization of the hot (top) and warm (bottom) CGM component for a fit with a free-to-fit background photon index versus a fit with the fixed photon index. This is for the 0.12 c/s hard rate cut and all errors are 90% confidence intervals. Fields are marked with different colors following Figure 7. Most fields are consistent between the two fits.

4 Discontinuity at 3 keV

Figure 2 exhibits a noticeable discontinuity at 3 keV. This feature is an effect of the hard rate cut (3-7 keV) applied to Halosat data and not due to a strange contribution to the spectra or instrumental effects. If a given hard band count rate cut is applied to the data, then the resulting spectrum will have a count decrement in that band compared to the adjacent energies, due to the independence of the uncertainties between the individual bins. We can actually see this effect in action simply by changing the energy band we base the cut on. Figure 10 shows the resulting set of stacked spectra if they are cut on 4-7 keV instead. There is no longer a feature at 3 keV, and instead a shift can be seen at 4 keV. This feature is most notable in spectra with large statistics, such as the stacked spectra, and is more noticeable for the stricter 0.12 c/s hard rate cut (see Figure 11).

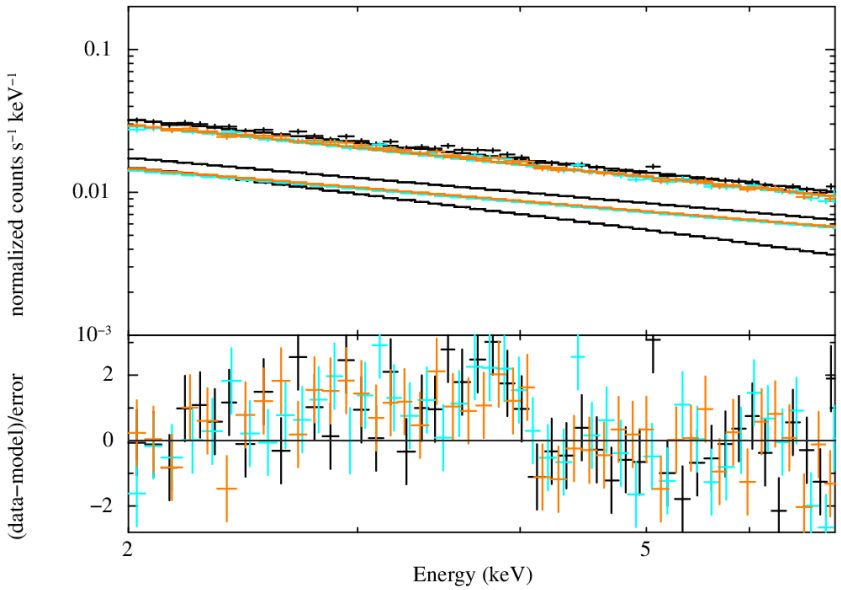

Figure 10: Stacked spectra (2-7 keV) using a 4-7 keV hard rate cut instead of a 3-7 keV hard rate cut. No discontinuity is present at 3 keV, instead there is a feature at 4 keV.

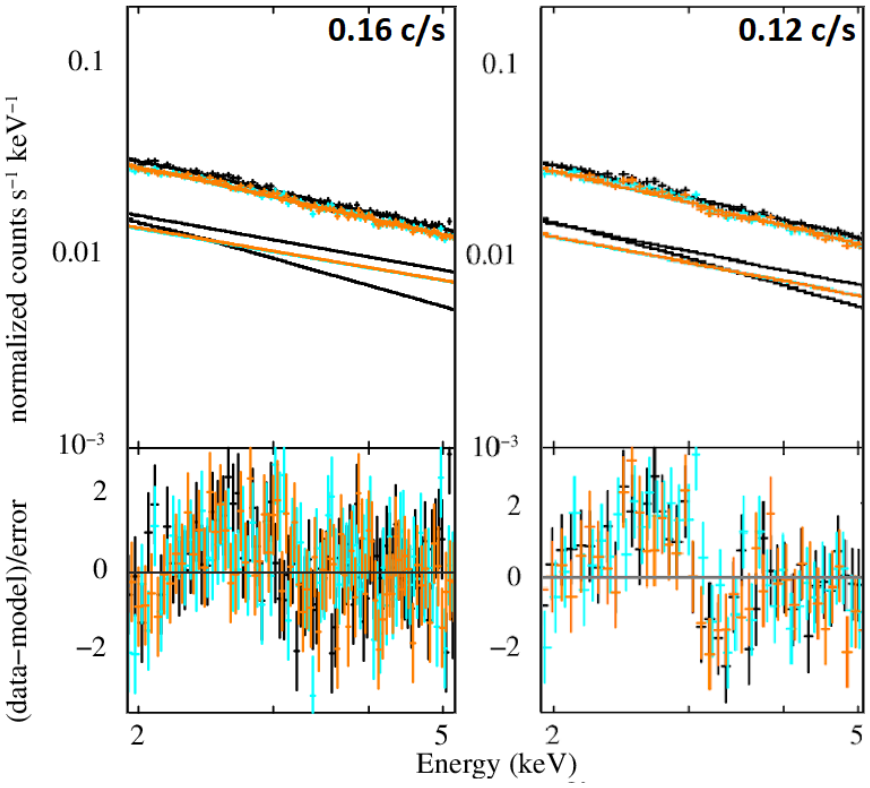

Figure 11: Comparing stacked spectra over a 2-5 keV energy range for the 0.12 c/s and 0.16 c/s hard rate cuts. Both feature the discontinuity at 3 keV due to the cut, but the discontinuity is more severe for the stricter rate cut.

5 Example Xspec script

The following section shows an example Xspec xcm script for loading and fitting the three HaloSat stacked spectra from Bluem et al. (2022). This script uses photon indices fixed to the median values from Table 1 as recommended, which is a small deviation from the original analysis in the published paper and the results shown in this document in Figure 2 and Table 2. This script was made for data using HaloSat software proc_ver hsuf_20200226, which requires the additional gain commands and an edge component in the model (Kaaret, P. & Bluem, J. Feb 2022, heasarc.gsfc.nasa.gov/docs/halosat/analysis/response20220128.pdf). The resulting spectra can be seen in Figure 12 and the fit parameters are in Table 3.

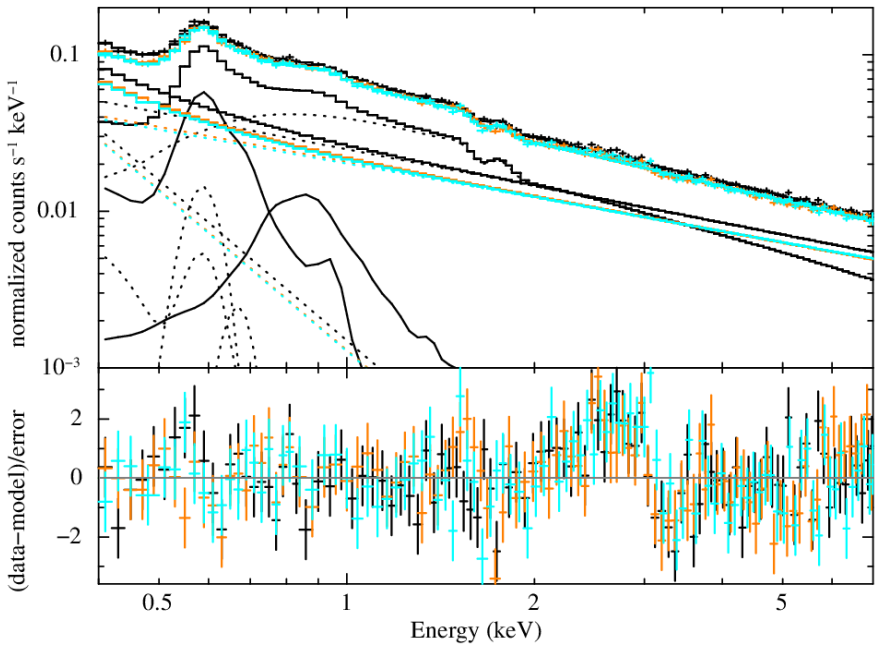

Figure 12: The stacked spectra from Bluem et al. (2022) fitted with fixed photon indices. Each HaloSat detector is a different color. The spectra have two components for the CGM, marked with solid black lines. Foreground and background components are marked with dashed lines. The instrument backgrounds are the two linear components, which can be seen with separate normalizations for the three detectors. The summed background contributions can be seen as the sweeping solid colored lines crossing the figure. The discontinuity at 3 keV is from the high-energy count rate cuts used and unrelated to the background (see Section 4).

model	parameter	value
Warm CGM APEC	kT (keV)	0.166 ± 0.005
	EM ($\mathrm{cm}^{-6}\,\mathrm{pc}$)	0.0131 ± 0.0008
Hot CGM APEC	kT (keV)	0.70 ± 0.04
	EM ($\mathrm{cm}^{-6}\,\mathrm{pc}$)	0.00137 ± 0.00013
Power law 1	normalization (DPU 14)	0.0249 ± 0.0003
	normalization (DPU 54)	0.0207 ± 0.0003
	normalization (DPU 38)	0.0202 ± 0.0003
Power law 2	normalization (DPU 14)	0.00149 ± 0.00016
	normalization (DPU 54)	0.00129 ± 0.00015
	normalization (DPU 38)	0.00127 ± 0.00014
Fit (DPU 14)	χ^2	361
Fit (DPU 54)	χ^2	370
Fit (DPU 38)	χ^2	345
Fit total	χ^2/DoF	1075/977

Table 3: Parameters of the model with fixed background photon indices fitted to the stacked spectra as shown in Figure 11. The Table is formatted similarly to Table 2.

Xspec script

```
data 1:1 stack_d14_dat.pi 2:2 stack_d54_dat.pi 3:3 stack_d38_dat.pi
response 1 hs_sdd_avgnoise20180701v001.rmf
response 2 hs_sdd_avgnoise20180701v001.rmf
response 3 hs_sdd_avgnoise20180701v001.rmf
arf 1 hs_sdd_all20180701v001.arf
arf 2 hs_sdd_all20180701v001.arf
arf 3 hs_sdd_all20180701v001.arf
response 2:1 hs_sdd_diag20180701v001.rmf
response 2:2 hs_sdd_diag20180701v001.rmf
response 2:3 hs_sdd_diag20180701v001.rmf
ign **:0.0-0.4
ign **:7.0-**
abund wilm
model (apec+TBabs*(pow)+TBabs*(apec+apec)+gauss+gauss)*edge
model 2:bg pow+pow
cpd /xw
setplot energy
setplot add
setplot rebin 12 6
gain 1 1 0.0232
gain 2 1 0.0239
gain 3 1 0.0240
newpar 1 0.084 -1
newpar 4 0.316 -1
newpar 5 0.0178 -1
newpar 6 1.45 -1
newpar 7 0.38 -1
newpar 8 0.0178 -1
newpar 9 0.69
newpar 10 0.3
newpar 12 0.11
newpar 13 0.166
newpar 14 0.3
newpar 16 1.11
newpar 17 0.5634 -1
newpar 18 0.001 -1
newpar 19 0.0322 -1
newpar 20 0.6531 -1
newpar 21 0.001 -1
newpar 22 0.00397 -1
newpar 23 1.83900 -1
newpar 24 -0.170,-1,-1.0,-1.0,1.0,1.0
newpar bg:1 0.80 -1
newpar bg:2 1
newpar bg:3 3.4 -1
newpar bg:4 1.1
newpar bg:5 0.75 -1
newpar bg:6 1.11
newpar bg:8 0.9
newpar bg:9 0.73 -1
newpar bg:10 1.01
newpar bg:12 1.00101
```